



Published in final edited form as:

Nat Commun. ; 5: 4930. doi:10.1038/ncomms5930.

Genetic deficiency of the mitochondrial protein PGAM5 causes a Parkinson's-like movement disorder

Wei Lu^{1,*}, Senthilkumar S. Karuppagounder^{2,3,4,*}, Danielle A. Springer⁵, Michele D. Allen⁵, Lixin Zheng¹, Brittany Chao¹, Yan Zhang⁶, Valina L. Dawson^{2,3,4,7,8}, Ted M. Dawson^{2,3,4,8,9}, and Michael Lenardo¹

¹Molecular Development of the Immune System Section, Laboratory of Immunology, National Institute of Allergy and Infectious Diseases, National Institutes of Health

²Neuroregeneration and Stem Cell Programs, Institute for Cell Engineering, Johns Hopkins University School of Medicine, Baltimore, MD 21205, USA

³Departments of Neurology, Johns Hopkins University School of Medicine, Baltimore, MD 21205, USA

⁴Adrienne Helis Malvin Medical Research Foundation, New Orleans, LA 70130-2685, USA

⁵Murine Phenotyping Core, National Heart, Lung, and Blood Institute, National Institutes of Health

⁶Molecular Mechanism of Apoptosis Section, Cell and Cancer Biology Branch, National Cancer Institute, National Institutes of Health

⁷Department of Physiology, Johns Hopkins University School of Medicine, Baltimore, MD 21205, USA

⁸Solomon H. Snyder Department of Neuroscience, Johns Hopkins University School of Medicine, Baltimore, MD 21205, USA

⁹Department of Pharmacology and Molecular Sciences, Johns Hopkins University School of Medicine, Baltimore, MD 21205, USA

Abstract

Mitophagy is a specialized form of autophagy that selectively disposes of dysfunctional mitochondria. Delineating the molecular regulation of mitophagy is of great importance because defects in this process lead to a variety of mitochondrial diseases. Here we report that mice deficient for the mitochondrial protein, phosphoglycerate mutase family member 5 (PGAM5), displayed a Parkinson's-like movement phenotype. We determined biochemically that PGAM5 is required for the stabilization of the mitophagy-inducing protein PINK1 on damaged mitochondria.

To whom correspondence should be addressed to: lenardo@nih.gov.

*These authors contributed equally to this work.

Contributions

W.L., S.S.K., designed and performed the experiments, analyzed the data and wrote the manuscript; D.A.S., M. D.A., Y.Z., B. C., and L.Z. did the experiments and analyzed the data; V.L.D., T.M.D., and M. L. designed the experiments, analyzed the data and wrote the manuscript.

Competing financial interests

The authors declare that there are no conflicts of interest.

Loss of PGAM5 disables PINK1-mediated mitophagy in vitro and leads to dopaminergic neurodegeneration and mild dopamine loss in vivo. Our data indicate that PGAM5 is a regulator of mitophagy essential for mitochondrial turnover and serves a cytoprotective function in dopaminergic neurons in vivo. Moreover, PGAM5 may provide a molecular link to study mitochondrial homeostasis and the pathogenesis of a movement disorder similar to Parkinson's disease.

Introduction

Mitochondria have a primary physiological role in producing ATP as an energy source, but also regulate cell survival^{1,2}. In response to cellular stress, dysfunctional mitochondria produce ROS and other pro-death mediators to initiate cell death programs, such as apoptosis, necroptosis, parthanatos, or autophagic cell death¹⁻⁵. Mitophagy, a selective form of autophagy, can target dysfunctional mitochondria for lysosomal degradation and protect cells from oxidative damage^{5,6}. Several regulators of mitophagy, including PINK1, Nix (BNIP3L), and parkin have been identified⁶⁻⁹. Mutations or deletions of these genes have been associated with abnormal mitophagy. Abnormal mitophagy has been observed in variety of diseases, including ischemic injury and neurodegenerative disease⁶⁻⁹. Hence, understanding the detailed mechanism of mitophagy remains an important goal for improving the diagnosis and treatment of diseases involving mitochondria.

Parkinson's disease is the second most common neurodegenerative disease and is characterized by the selective loss of dopaminergic neurons⁹⁻¹¹. Although the cause of death of dopamine-secreting neurons is still debated, oxidative stress originating from mitochondria and mitophagy defects have been proposed to contribute to disease pathogenesis^{12,13}. Two autosomal recessive Parkinson's disease genes, PINK1 (PTEN induced putative kinase 1) and parkin, can regulate mitophagy¹⁴. PINK1 is a cytosolic and mitochondrion-associated kinase that is continuously degraded in healthy cells by mitochondrial proteases, including the mitochondrial inner membrane protease Presenilin-associated, rhomboid-like (PARL) protein^{15,16}. Mitochondrial membrane depolarization inhibits PINK1 degradation, causing it to accumulate and promote mitophagy via recruitment of another familial Parkinson's protein, the E3 ubiquitin ligase, parkin^{17,18}. However, the detailed mechanism of PINK1 degradation and stabilization remains unclear. PINK1 is mutated in autosomal recessive early-onset Parkinson's disease¹⁹⁻²¹, but many putative pathogenic mutations are found in heterozygous individuals or even in healthy controls²⁰, which suggests that it is important to identify other critical factors for the protective effect of PINK1 against dopaminergic degeneration.

PGAM5, paralog member 5 of a family of highly-conserved phosphoglycerate mutases, is a 32 kD mitochondrial protein that apparently lacks phosphotransfer function on phosphoglycerates, but retains activity as a serine/threonine protein phosphatase that regulates the ASK1 kinase²². The functions of PGAM5 are complex since it also serves as an anti-oxidant regulator in the Kelch ECH associating protein 1-nuclear factor-E2-related factor 2 (KEAP1-NRF2) signaling pathway and binds Bcl-X_L^{23,24}. Recently, PGAM5 was described as a downstream target of RIP3 responsible for recruiting the RIP1-RIP3-MLKL

necrosis “attack” complex to mitochondria^{4,25}. Interestingly, PGAM5 has also been reported as a genetic suppressor of PINK1 in *Drosophila*²⁶, as well as a substrate of PARL²⁷. Thus, it is important to establish the *in vivo* role of PGAM5 in mitochondrial disease pathogenesis. Here we show PGAM5 is a new mitophagy regulator in the PINK1/parkin pathway, and that genetic deficiency of PGAM5 in mice causes a Parkinson’s disease-like phenotype.

Results

PGAM5 is a novel regulator of PINK1/parkin regulated mitophagy pathway

We generated *Pgam5* knockout (KO) mice from gene targeted embryonic stem cells and verified that homozygotes exhibited a nearly complete loss of *Pgam5* mRNA as well as protein expression (Supplementary fig. 1). Because of our interest in mitochondrial regulation, we examined mouse embryonic fibroblasts (MEFs) by transmission electron microscopy (TEM). We observed that KO MEFs contained an increased number of swollen bulbous mitochondria that lacked normal cristae and were filled with non-descript granular debris that were not found in wild-type (WT) MEFs (Fig. 1a, and supplementary fig. 2a). Moreover, KO MEFs manifested constitutively elevated levels of intracellular ROS and a subtle decrease in the mitochondrial potential measured by the dye TMRE, which indicates stressed or damaged mitochondria⁴ (Supplementary fig. 2b and c). We hypothesized that PGAM5 promotes the clearance of unhealthy or damaged mitochondria to maintain mitochondrial homeostasis through mitophagy. We therefore examined *Pgam5* KO MEFs treated with carbonyl cyanide *m*-chlorophenyl hydrazine (CCCP), which exacerbates mitochondrial stress and mitophagy by uncoupling the mitochondrial proton gradient essential for oxidative phosphorylation^{17,18}. After CCCP treatment, WT MEFs showed an increase in double-membrane vesicles, a decrease in mitochondria, and some mitochondria encapsulated by a double-membrane structure characteristic of mitophagy (Fig. 1b). By contrast, TEM of KO MEFs revealed increased numbers of swollen unhealthy mitochondria but double-membrane vesicles-encapsulated mitochondria were absent (Fig. 1b and quantification in supplementary fig. 2d). CCCP treatment also increased ROS levels and decreased mitochondria membrane depolarization to a greater extent in KO compared to WT cells consistent with failed mitophagy (Supplementary fig. 2e and f).

We next performed biochemical analyses of mitophagy and found that although the microtubule-associated protein 1A/1B light chain 3 (LC-3) was processed from LC-3I to LC-3II, in both WT and KO MEF cells after 3 or 6 hours of CCCP treatment, the autophagic removal of cytosolic sequestosome 1 (p62), was markedly impaired in KO MEFs (Fig. 1c)²⁸. With longer CCCP exposure (12 hrs), KO MEFs showed reduced mitochondrial clearance as indicated by the persistence of COX IV, an inner mitochondrial membrane (IMM) protein and Tomm20, an outer mitochondrial membrane (OMM) protein in total cell lysates (Fig. 1d). We directly visualized mitophagy using mt-Keima, an IMM-targeted fluorescent protein resistant to lysosomal proteases whose excitation fluorescence (λ_{ex}) is 450 nm (green fluorescence) at neutral pH in the cytosol and shifts to 550 nm (red fluorescence) at acid pH following delivery of mitochondria to acidic lysosomes²⁹. We observed that CCCP treatment of WT MEFs induced the expected shift of mt-Keima from

an evenly distributed green mitochondrial appearance to a bright red punctate appearance, indicating relocation of mitochondria to acidic autolysosomes by mitophagy (Fig. 1e, left panels). By contrast, *Pgam5* KO cells exhibited persistent green fluorescence and very little red punctate fluorescence revealing a severe defect in mitophagy (Fig. 1e, right panels, and quantification in Supplementary fig. 2g). Hence, PGAM5 is apparently indispensable for the process of mitophagy.

Since PINK1 is a well-known mitophagy protein that binds PGAM5^{8,26}, we tested its function in *Pgam5* KO MEFs. We observed that purified mitochondria from WT cells treated with CCCP for 3 hr exhibited dramatic stabilization of the 63 kD full-length PINK1 protein but this effect was completely abolished in *Pgam5* KO cells (Fig. 1f). Lentiviral-mediated expression of GFP-tagged PGAM5 in KO MEFs fully rescued PINK1 indicating that PGAM5 accounted for PINK1 mitochondrial stabilization (Supplementary fig. 3). We found that shRNA knock-down of *PGAM5* in HeLa cells also disrupted PINK1 stabilization on the OMM after CCCP treatment (Fig. 1g). Notably, we also observed that CCCP shifted PGAM5 to a predominantly faster migrating species suggesting proteolytic cleavage in the mitochondria (Fig. 1f and g). Finally, parkin, which is recruited by PINK1 to assist mitophagy, was not influenced by the knock-down of PGAM5 under normal conditions (Fig. 1h). However, after CCCP treatment, parkin exhibited defective mitochondrial translocation and remained diffuse, likely due to impaired PINK1 stabilization and recruitment (Fig. 1i and j for quantification).

PGAM5 protects PINK1 from IMM degradation

To investigate how PGAM5 regulates PINK1 stability, we first examined the phosphatase function of PGAM5¹⁹. We introduced a phosphatase-dead mutant (H105A) of PGAM5 into WT and KO MEFs and found that both the mutant and unaltered forms restored PINK1 stabilization following CCCP treatment indicating that PGAM5 phosphatase function was not essential (Supplementary fig. 4). We noticed that N-terminal and C-terminal tagged PGAM5 protein showed two bands or one band, respectively, when exogenously expressed in HEK293T cells, confirming proteolytic cleavage occurs close to its N-terminus (Supplementary fig. 5). In purified mitochondria from WT MEFs, we observed two endogenous PGAM5 bands, a 32 kD band corresponding to full length PGAM5, and another 3 kD smaller consistent with previous observations that PGAM5 can be cleaved in the TM (Fig. 2a left panel)²⁷. Examining MEFs from mice genetically deficient in PARL, an IMM rhomboid protease, we observed that purified mitochondria only contained full-length PGAM5 confirming that it is a substrate of the IMM protease PARL and that PGAM5 is localized to the IMM (Fig. 2a, right panel)²⁷. We further confirmed the IMM location of PGAM5 by exposing purified mitochondria to increasing doses of proteinase K, which degrades outer membrane proteins such as Tomm20. PGAM5 resisted proteinase K degradation confirming an IMM location (Fig. 2a)²⁷. Previously it has been shown that PINK1 undergoes cleavage by PARL and turnover in the IMM in healthy mitochondria¹⁵. Therefore, our data implied that PGAM5 facilitates stabilization of PINK1 against PARL cleavage in the IMM after CCCP exposure. This inference was strengthened by an experiment in which PARL expression was reduced by a small hairpin RNA (PARLsh) and

we found that PINK1 was stabilized even in PGAM5 KO mitochondria following CCCP treatment (Fig. 2b, and supplementary fig. 6).

We therefore examined the ability of PGAM5 to stabilize WT PINK1 as well as a variety of PINK1 mutant alleles causing recessive early-onset Parkinson's disease. We co-expressed epitope-tagged versions of PGAM5 and PINK1, we found that the presence of PGAM5 dramatically increased the level of full-length WT PINK1 (*63KD) and decreased the PARL-cleaved form of PINK1 (#54KD) (Fig. 2c). By contrast, co-expression with a GFP control protein left WT PINK1 as a weak full-length band together with smaller PARL cleaved bands (Fig. 2c, compare lanes 1 with 10 in which the ratios of the 63 kD to 54 kD PINK1 forms were 6.8 and 0.14, respectively)¹⁵. However, the Parkinson-associated mutant forms of PINK1 exhibited poor stability and varied cleavage patterns (Fig. 2c, lanes 11–18). Moreover, PGAM5 overexpression failed to increase the accumulation of full-length versions of the mutant proteins with the possible exception of 309 (Fig. 2c, lanes 2–9). The stabilization of PINK1 by PGAM5 in this co-expression assay is not affected by CCCP treatment (Supplementary fig. 7). Therefore, Parkinson-associated PINK1 mutants are generally resistant to PGAM5 stabilization.

We tested the mechanism of stabilization by examining the importance of direct association of PGAM5 with PINK1. We found that myc-tagged PGAM5 co-precipitated PINK1 in HEK293T cells and this was moderately diminished by CCCP treatment (Fig. 2d). Co-immunoprecipitation of fragments of PGAM5 with GFP-tagged PINK1 demonstrated that the 1 to 110 fragment or the 98 to 289 fragment bound PINK1, but the 1 to 98 fragment did not, implying that residues 98 to 110 of PGAM5 were important for binding (Fig. 2e). Alignment of PGAM5 amino acid sequences from different species showed that this region (98-110) is highly evolutionarily conserved with an amino acid motif consisting of two RH dipeptides precisely separated by four hydrophobic amino acids (the “di-RH” motif) (see Supplementary fig. 8 for a protein sequence alignment). We therefore created amino acid substitutions of either both arginines (2R) or both histidines (2H) with alanine and expressed these two PGAM5 mutants 2RA (R98A/R104A) and 2HA (H99A/H105A) at equivalent levels to the WT protein and tested for PINK1 stabilization. We found the 2RA mutation lost essentially the entire PINK1 stabilization function (Fig. 2f) and the corresponding immunoprecipitation experiment showed that PGAM5 2RA completely lost the ability to bind to PINK1 (Fig. 2f). Furthermore, we found that the 2H mutant showed a partial loss of PINK1 stabilization and a corresponding partial loss of association with PINK1 (Fig. 2f). This supports the view that direct association between PGAM5 and PINK1 is crucial for the stabilization of the latter protein and also demonstrates that the di-RH motif is important for this association.

Notably, PINK1 stabilized on purified mitochondria by CCCP treatment becomes sensitive to exogenously added proteases implying that it traffics to the OMM whereas PGAM5 is protected implying that remains in the IMM (Supplementary fig. S9). This could account for the partially diminished binding of PINK1 to PGAM5 after CCCP treatment (Fig. 2d). We therefore assessed PINK1 topology by transfecting PINK1 with or without PGAM5 into HEK293T cells and then gently permeabilizing the plasma membrane with digitonin, which does not compromise the OMM or IMM³⁰. We then added trypsin, which diffuses into the

behavioral phenotype of *Pgam5* KO mice reveals some, but not all Parkinson's disease features.

PGAM5 deficiency causes mouse Dopamine neuron degeneration

To determine whether the abnormal movement phenotype in *Pgam5* KO mice might be due to dopaminergic dysfunction, we examined dopamine (DA), and its metabolites dihydroxyphenylacetic acid (DOPAC), 3-methoxytyramine (3-MT) and homovanillic acid (HVA) neurochemistry in striatal lysates by high-performance liquid chromatography-electrochemical detection (HPLC-ECD in mice at 1 month, 2 months and 12 months of age). We observed that the KO and WT mice showed no difference in neurotransmitter levels at 1 month of age. Starting from 2 months old, we found a mild but significant decrease of DA content in KO compared to WT mice (Fig. 5a). The DA and its metabolic product of DOPAC were also significantly reduced in 12-month old KO mice (Fig. 5b). However, the levels of other metabolites of 3-MT and HVA, were equivalent in KO and WT animals at all time points (Fig. 5c and d). To analyze whether the catabolism of DA is altered in WT versus KO mice, we calculated the DA turnover ratio and we observed no significant changes in any time point (Supplementary fig 11a and b). Further analyses also did not show any significant changes in serotonin (5HT), 5-hydroxyindoleacetic acid (5HIAA) and 5HT turnover ratio (Supplementary fig. 11c–e).

To investigate the effect of PGAM5 deficiency on DA neuron viability, we quantified tyrosine hydroxylase (TH) immunoreactivity and Nissl staining in the substantia nigra pars compacta (SNpc) and ventral tegmental area (VTA) by an unbiased stereological method. WT and KO mice exhibited no difference in TH positive or Nissl stained neurons number at 1 month old, which indicates that early development is normal in the absence of PGAM5. At 2 months of age there is a trend toward the loss of TH-positive and Nissl stained neurons. At 12 months of age we observed a significant loss of TH-positive (43%) and Nissl (35%) stained neurons in the SNpc (Fig. 5e–g). Stereological counts from the VTA did not show any significant changes in TH and Nissl positive neurons at any age (Supplementary fig. 11f, and g). Thus, VTA DA neurons are less sensitive than SNpc DA neurons to the absence of PGAM5, which is similar to the differential vulnerability of these DA neurons in Parkinson's disease.

L-3,4-dihydroxyphenylalanine (L-DOPA) is the precursor of dopamine and an effective treatment to rescue the behavioral abnormalities in Parkinson' disease. We administered L-DOPA to 18-month old WT and KO mice, and observed increased mobility and activity in KO mice in the Open-Field test. We found a mild increase in the movement of the WT mice (probably due to the high dose of L-DOPA injected into aged mice), but a much more significant improvement in the mobility and activity of the KO mice after treatment with L-DOPA (Fig. 6a and b). We also evaluated other regions of the brain from *Pgam5* KO mice. No obvious general neurodegeneration was observed in the cortex, hippocampus, or cerebellum (Supplementary fig. 12). Collectively, these data indicate that the abnormal behavior phenotype of the KO mice likely involves the documented loss of SNpc DA neurons. Finally, we evaluated heart tissue from *Pgam5* KO mice, since PINK1 has been reported to be important for heart function³⁵. We did not observe a mitochondrial

abnormality in heart tissue by TEM in PGAM5 KO mice (Supplementary fig. 13). Thus, mice genetically deficient in PGAM5 exhibit a specific neurological abnormality related with progressive loss of SNpc DA neurons, which mimics a Parkinsonian-like behavioral phenotype.

Discussion

Our studies have shed new light on the mechanism of PINK1 stabilization by unveiling a new function of the mitochondrial regulatory protein PGAM5. PINK1 stabilization and subsequent parkin recruitment triggers mitophagy, which selectively eliminates dysfunctional mitochondria to protect cells/tissues from oxidative stress and cell death^{13,14}. Here we provide new evidence suggesting that mitophagy may contribute to dopaminergic neurodegeneration and movement disorders in experimental animals by the role of PGAM5 in these processes. PINK1 and parkin also regulate mitochondrial quality control through other pathways including mitochondria fusion/fission and biogenesis, to which PGAM5 may also contribute^{36,37}. Contrary to a previous study in drosophila²⁶, we found PGAM5 protects dopamine neurons from degeneration, presumably by promoting PINK1 stabilization. Consistent with a mitochondrial pathogenesis for Parkinson's disease, PINK1 deficiency in drosophila causes energy depletion, shortened lifespan, and dopamine neuron degeneration^{38,39}. Aged *Pink1* deficient mice show impaired neural activity similar to *Pgam5* KO mice, but without DA neurodegeneration²⁹; and mutations in PINK1 and parkin predispose to the movement disorders and DA neurodegeneration that characterizes familial Parkinson's disease in humans¹⁷. The new role for the mitochondrial protein PGAM5 in dopamine neuron pathology, lends further weight to the mitochondrial theory of Parkinson's pathogenesis.

The *Pgam5* KO mice showed a clear movement disorder at one year of age, as well as significant dopaminergic neurodegeneration at an even earlier age. However, the magnitude of DA loss in *Pgam5* KO mice is very small. In humans and in MPTP-treated mice, a loss of at least 75–80% of the dopamine neurons is required for locomotor problems to be exhibited⁴⁰. The relatively small decrease of DA may due to the compensatory secretion of DA from remaining DA neurons in SN or VTA. Another possibility is that the movement disorder phenotype may also result from dysfunctional DA neurons, a decrease of DA receptor sensitivity or other neurotransmitter systems, which have not yet been identified in *Pgam5* KO mice.

An important question is why *Pgam5* KO mice apparently show a more severe phenotype than the PINK1 KO mouse^{31,32}. We hypothesize that the difference between *Pink1* KO and *Pgam5* KO may be due to microbiome differences, uncontrolled environmental variables or genetic background differences. Recent discoveries clearly showed that mouse microbiota modulate neuron development⁴¹. Mice from different facilities and vendors also bear quite different intestinal microbiota⁴², which may influence the assessment of neurological function. Mouse genetic background also impacts the results of mouse KO models, since the accumulation of homozygous mutations during the inbreeding may disrupt proteins whose function is important for the evaluated mouse phenotype. For example, a point mutation in C56Bl6/N inbred mice strain attenuates the sensitivity to cocaine responses⁴³. Moreover, the

Author Manuscript

Author Manuscript

Author Manuscript

autonomous deletion of *Casp11* in strain 129 mice reduces inflammasome activation compared to C57Bl6 strain⁴⁴. Alternatively, the different outcomes may be due to the lack of compensatory mechanisms in the *Pgam5* KO mice, which are active in *Pink1* KO mice. We remain open to the possibility that PGAM5 may regulate other factors essential for dopamine neuron survival independent of the PINK1/parkin pathway. We have not observed any direct effect of PGAM5 on the mitochondrial import mechanism, however, there may be indirect effects on import as well as on the mitochondria fission/fusion system regulated by Drp1²⁵. Previous reports have mentioned, and we also confirmed (data not shown), that PGAM5 strongly interacts with KEAP1, which is an adaptor protein for E3 ubiquitin ligase CUL3. PGAM5 can help release NRF2 from KEAP1, in order to facilitate NRF2 regulated anti-oxidant gene expression. Lack of PGAM5 disrupts both PINK1/parkin mediated mitophagy and the NRF2-regulated anti-oxidant response, which could account for the dopamine neuron degeneration²³. These additional factors might explain why dopamine neurodegeneration is absent in *Pink1/Parkin* knockout mice but present in the *Pgam5* KO mice.

Homozygous recessive and compound heterozygote mutations in PINK1 have been identified in 1–2% of early-onset Parkinson's disease patients⁴⁵. PGAM5 mutations have not yet been reported in any human disease and whether PGAM5 mutations can be found in unexplained familial Parkinson's disease patients now becomes a question of great interest. Patients with germline mutations in PINK1 or parkin show a restricted degeneration of DA neurons with no general neurodegeneration or abnormalities in other tissues. *Pgam5* KO mice show an analogous restricted phenotype. It is unclear why only DA neurons, rather than other types of cells, are sensitive to the PINK1/parkin mutations or PGAM5 deficiency. The fact that DA neurons require energy generated from mitochondria and that DA neurons in SNc are quite sensitive to the oxidative stress generated from mitochondria might explain why maintaining healthy mitochondria is crucial for DA neuron viability⁴⁶. PGAM5 deficiency fails to scavenge oxidative stress and abnormal mitochondria, which apparently leads to specific dopaminergic neuron degeneration.

In conclusion, our data indicate that PGAM5 is a new regulator of mitophagy essential for mitochondrial turnover and a key determinant of dopamine neuron survival in vivo. The *Pgam5* KO mouse may be useful for the development of diagnostic tests and drug discovery for Parkinson's disease in the future.

Materials and Methods

Mice and cells

Author Manuscript

Validated *Pgam5* gene-targeted ES cells (B6 background: JM8.N4) were purchased from the European Mouse Mutant Cell Repository and chimeric mice were derived by microinjection of ES cells into blastocyst donors. *Pgam5* KO mice were generated by breeding chimeric animals (Laboratory Animal Service Program of NCI-Frederick). *Pgam5* WT and KO mice were bred and maintained in NIH animal facility at SPF (Specific Pathogen Free) conditions. Mouse experiments were carried out in accordance with NIAID Animal Care and Use Committee guidelines under an approved protocol. 12-month old female mice were used in all the animal study unless specifically indicated. MEF cells were prepared from day

12.5 embryos and cultured in DMEM/F12 full media (FM) (FM: 10% fetal bovine serum, 4 mM L-glutamine, 100 IU ml⁻¹ penicillin, and 100 mg ml⁻¹ streptomycin) plus non-essential amino acids. Bone marrow cells were cultured in RPMI FM plus 20 ng ml⁻¹ mouse M-CSF (Biolegend) for 7 days to induce macrophage differentiation. *Parl* WT and KO MEFs are from Dr. Bart De Strooper (Center for Human Genetics, Flanders Interuniversity Institute for Biotechnology (VIB4) and K.U. Leuven, Leuven, Belgium).

Antibodies, siRNA and primers

The homemade PGAM5 antibody was made against the peptide, CGSLEKDRTLPLGR by Genscript (NJ, USA). Commercial PGAM5 Antibody was purchased from Abcam (Ab126534). Mouse PINK1 and PARL (Sigma); Human PINK1 (Novus) and LC-3, COXIV, VDAC, Actin, HSP60 and myc-tag antibodies (Cell Signaling Technology). Primary antibodies were used at 1:1000 dilution in 5% non-fat milk, while HRP-labeled secondary antibodies (Southern Biotech) were used at 1:4000 dilution.

PGAM5 siRNA sequence: ACGCGCGCCAUAGAGACCACCGAUA (Life Technology, stealth siRNA). *Pgam5* real-time PCR primers, forward: ATCTGGAGAAGACGAGTTGACA; reverse: CCTGTTCCCGACCTAATGGT.

Lentiviral shRNA-mediated knockdown and cDNA overexpression

pLKO.1 *PGAM5* shRNA plasmids were purchased from OpenBiosystem/Thermo Scientific. MEF cells were infected with lentivirus encoding shRNA against *PGAM5* for 24 hours before selection with 10 µg ml⁻¹ puromycin according to the manufacturer's specifications. The *PGAM5* sequence was cloned into bicistronic lentiviral GFP vectors (Abmgood). GFP control virus and *PGAM5*-GFP lentivirus were used to transduce MEF cells followed by puromycin selection as above.

Western blot

Cells were collected and lysed in buffer (20 mM Tris/HCl, pH 7.2, 0.5% (v/v) Nonidet P-40, 300 mM NaCl, 3 mM EDTA, 3 mM EGTA, 2 mM dithiothreitol, 2 mM PMSF, 100 µM leupeptin, 10 µM bestatin, 10 µM pepstatin and 2 µg ml⁻¹ of aprotinin). Supernatants were collected after centrifugation at 10,000 x g for 20 min at 4° C, separated by 4–20% SDS-PAGE and analyzed by immunoblot. Cells and tissue mitochondria were purified by using Qproteome mitochondria isolation Kit (Qiagen). The mitochondria pellet was then lysed in 2 x SDS loading buffer and loaded onto SDS-PAGE gels for western blot. The quantification of western blot bands as well as representative examples of uncropped western blots are included in Supplementary fig. 14).

Live cell imaging

MEFs stably transduced with lentivirus encoding mitochondria targeted Keima protein (mtKeima) were cultured in glass-bottom dishes (MatTek). Cells were always kept around 50% confluency before any treatment. Cells were treated with 20 µM CCCP for 24 hr and then scanned and images were collected on a Leica TCS-NT/SP confocal microscope (Leica Microsystems, Exton, PA USA) using a 40 x oil immersion objective NA 1.32. Detector slits were configured to minimize any cross-talk between the channels. Images were

processed using the Leica TCS-NT/SP software (version 1.6.587), Imaris 3.2 (Bitplane AG, Zurich Switzerland), and analyzed and quantified by Image J software.

Trypsin protection assay

Transfected cells or purified mitochondria were re-suspended in cold Hank's balanced salt solution or mitochondria storage buffer (Qiagen mitochondria isolation kit). Cells were firstly treated 20 μ M digitonin or 0.05% Triton X-100 for 1 minute, and then cells (or purified mitochondria) were incubated with different concentrations of trypsin on ice for 30 minutes. 6 X SDS loading dye was added to stop the reaction and lyse the cells (mitochondria) for western blot analysis.

Behavior Tests

The movement of *Pgam5* KO and WT mice (WT n=10, KO n=8, all female, 12-month old) was assessed in an open field chamber. Mice were individually placed in a 50 \times 50 cm square arena with 50 cm high black opaque plastic walls. The movement and activity of the mice were recorded for 60 minutes using a ceiling mounted video camera and a video mouse behavioral tracking system (Anymaze, Stoelting Co, Illinois). The open field tests were performed during the dark phase of the light cycle.

For gait assessment, video recordings of the underside of mice ambulating at a constant speed (13 cm s^{-1} and 18 cm s^{-1}) were obtained using a transparent treadmill belt positioned above a high-speed digital camera (DigiGait Imaging System, Mouse Specifics, Boston MA). Video captures of 3–4 continuous seconds in which the mice walked without stumbling and maintained a consistent position on the belt for a minimum of 10 consecutive strides were subsequently analyzed for multiple spatial and temporal gait parameters through the DigiGait Image Analysis System software. The DigiGait Imaging and Analysis system is based on ventral plane videography, and proprietary software that digitizes paw images and calculates the areas of approaching and retreating paws relative to belt and camera frame by frame as previously described^{47, 48}.

Motor coordination was evaluated with using a Rotamex-5 four lane Rotarod (Columbus Instruments, Columbus OH) consisting of a 3 cm diameter ridged plastic rotary rod positioned 60 cm above the table. On day 1, the mice were acclimated to the testing environment by placing them on the stationary rotary rod. The mice received three 60 sec acclimation trails separated by a one hour rest interval. Mice were trained on a rotating rod starting the same afternoon by habituation to a slowly rotating rod (5 rpm) for three 120 sec trials with a one hour rest interval and on day 2 they received three 120 sec training trials at the fixed speeds of 8 rpm in the morning and 10 rpm in the afternoon. The testing phase occurred 24 hours after training. The mice were tested for two days at fixed rotation speeds, receiving three 120 second trials with one hour rests intervals between trials. On day 1 they were tested at 8 rpm, followed by 10 rpm in the afternoon, and on day two they were tested at 12 rpm in the am and 15 rpm in the afternoon. On day three the mice were placed on a rod programmed to accelerate from 4–40 rpm. The testing session consisted of three 300 sec trials separated by 1 hour rest intervals. Testing was spaced out over multiple days to prevent fatigue, or handling stress to confound the testing results. Latency to fall off the

rotating rod was detected by photo-detectors and automatically recorded along with the acceleration speed at the time of falling.

Balance and coordination was also investigated using the vertical pole test as described by Matsuura et al.⁴⁹. Briefly, the mice were placed head up on a 50 cm high, 10 cm diameter vertical pole. The time for the mice to turn to a head downward position and the time to descend the pole were recorded and averaged over three trials

A number of neuromuscular phenotyping screens were also performed including the observation of rearing behavior of mice placed in a transparent glass walled enclosure during a 90 sec observational trial, the adhesive dot removal test in which the average time to remove a sticker placed on the snout was recorded over three trials, the akinesia test for the detection of mobility deficits as assessed by the latency to move all four limbs after placement onto a flat surface, and a catalepsy test to assess the ability of the mice to correct an abnormally imposed body position after placement of the hind limbs on a raised 1.5 inch block by the experimenter. Lastly, the mice were timed as they performed a ladder traversal test. The average time to cross a 30 cm long metal grid, with horizontally oriented bars placed 1.25 cm apart and positioned vertically at a 50 degree angle was calculated over three trials. All animal experiments were performed in accordance and with approval from the NHLBI and NIAID Animal Care and Use Committee.

Monoamine Analysis

Biogenic amine concentrations were measured by high-performance liquid chromatography with electrochemical detection (HPLC-ECD)⁴⁸. Briefly, mice were sacrificed by decapitation and the striatum was quickly removed. Striatal tissue was weighed and sonicated in 0.2 ml ice cold 0.01 mM perchloric acid containing 0.01 % EDTA and 60 ng 3,4-dihydroxybenzylamine (DHBA) as an internal standard. After centrifugation (15,000 × g, 30 min, 4°C), the supernatant was passed through a 0.2 μm filter. Twenty microliters of the supernatant were analyzed in the HPLC column (3 mm x150 mm C-18 reverse phase column, Acclaim™ Polar Advantage II, Thermo Scientific, USA) by a dual channel coulochem III electrochemical detector (Model 5300, ESA, Inc Chelmsford, MA, USA). The protein concentrations of tissue homogenates were measured using the BCA protein assay kit (Pierce, Rockford, IL, USA). Data were normalized to protein concentrations and expressed in ng ug⁻¹ protein.

Immunohistochemistry and quantitative analysis

Mice were perfused with ice-cold phosphate buffered saline (PBS) followed by 4% paraformaldehyde/PBS (pH 7.4). Brains were removed and post-fixed for 4 hrs in the same fixative. After cryoprotection in 30% sucrose/PBS (pH 7.4), the brains were frozen and serial coronal sections (60 μm sections) were cut with a microtome. Free-floating 60 μm sections were blocked with 5 % goat serum/PBS plus 0.2% Triton X-100 and incubated with an antibody against TH (rabbit polyclonal; Novus Biologicals) followed by incubation with biotin-conjugated anti-rabbit antibody (anti-rabbit polyclonal; Vector Labs), ABC reagents (Vector Labs), and SigmaFast DAB Peroxidase Substrate (Sigma-Aldrich). Sections were counterstained with Nissl (0.09 % thionin).

As described before⁵⁰, TH-positive cells and Nissl from the SNpc and (Ventral tegmental area) VTA region were counted through optical fractionators, the unbiased, 3-dimensional method for cell counting. This method was carried out by using a computer-assisted image analysis system consisting of an Axiophot photomicroscope (Carl Zeiss Vision) equipped with a computer controlled motorized stage (Ludl Electronics), a Hitachi HV C20 camera, and Stereo Investigator software (MicroBright-Field). The total number of TH-stained neurons and Nissl counts were calculated.

Benserazide and L-DOPA treatment

Nine 18 month-old WT, and *Pgam5* KO mice were divided into two groups receiving either intraperitoneal injections of 12.5 mg kg⁻¹ benserazide (Sigma) 20 min before receiving intraperitoneal injections of 5 mg kg⁻¹ L-DOPA (Sigma) or two injections of water separated by 20 min. Behavioral testing began 20 min after the L-DOPA injection⁵¹.

Statistical analysis

All histology quantitative data are expressed as the mean \pm SEM. Statistical significance was determined by two-way ANOVA followed by Bonferroni post-hoc analysis for comparison among multiple treatment groups. *p* values lower than 0.05 were considered to be significant. Respective *p* values are indicated in figure legends. *Asterisks sign indicate statistical significance between WT versus *Pgam5* KO mice.

Acknowledgments

The authors thank Drs. Toren Finkel, Chrysi Kanellopoulou, and Zhihua Liu for advice and help. We also thank Drs. Rebecca Baker, Ronald Germain, Carrie Lucas, Richard Siegel, Helen Su, Stefan Muljo, Chrysi Kanellopoulou and Qian Zhang for critically reading the manuscript and Dr. Bart De Strooper for providing *Parl* knockout MEFs. We also thank Bryan Hansen and Elizabeth Fisher for electron microscopy services and Sundar Ganesan and Juraj Kabat for bio-imaging assistance through NIAID core facilities. We thank Richard Youle, Michael Lazaro, and Danielle Sliter for help with the mitophagy experiments.

This work was supported in part by the Intramural Research Programs of the National Institute of Allergy and Infectious Diseases, National Heart Lung and Blood Institute, National Institutes of Health, and a grant from the National Institutes of Health/National Institute of Neurologic Disorders and Stroke NS38377 (SSK, VLD, TMD) and the JPB Foundation (TMD). The authors acknowledge the joint participation by the Adrienne Helis Malvin Medical Research Foundation (SSK, VLD, TMD) through their direct engagement in the continuous active conduct of medical research in conjunction with The Johns Hopkins Hospital and the Johns Hopkins University School of Medicine and the Foundation's Parkinson's Disease Program. TMD is the Leonard and Madlyn Abramson Professor in Neurodegenerative Diseases.

References

1. Galluzzi L, Kepp O, Kroemer G. Mitochondria: master regulators of danger signalling. *Nat Rev Mol Cell Biol.* 2012; 13:780–788. [PubMed: 23175281]
2. Vafai SB, Mootha VK. Mitochondrial disorders as windows into an ancient organelle. *Nature.* 2012; 491:374–38. [PubMed: 23151580]
3. Yu L, et al. Regulation of an ATG7-beclin 1 program of autophagic cell death by caspase-8. *Science.* 2004; 304:1500–1502. [PubMed: 15131264]
4. Kaczmarek A, Vandenabeele P, Krysko DV. Necroptosis: the release of damage-associated molecular patterns and its physiological relevance. *Immunity.* 2013; 38:209–223. [PubMed: 23438821]
5. Wang Y, Dawson VL, Dawson TM. Poly(ADP-ribose) signals to mitochondrial AIF: a key event in parthanatos. *Exp Neurol.* 2009; 218:193–202. [PubMed: 19332058]

6. Gottlieb RA, Carreira RS. Autophagy in health and disease. 5. Mitophagy as a way of life. *Am J Physiol Cell Physiol*. 2010; 299:C203–210. [PubMed: 20357180]
7. Kubli DA, Gustafsson Å. Mitochondria and mitophagy: the yin and yang of cell death control. *Circ Res*. 2012; 111:1208–1221. [PubMed: 23065344]
8. Youle RJ, Narendra DP. Mechanisms of mitophagy. *Nat Rev Mol Cell Biol*. 2011; 12:9–14. [PubMed: 21179058]
9. Savitt JM, Dawson VL, Dawson TM. Diagnosis and treatment of Parkinson disease: molecules to medicine. *J Clin Invest*. 2006; 116:1744–1754. [PubMed: 16823471]
10. de Lau LM, Breteler MM. Epidemiology of Parkinson's disease. *Lancet Neurol*. 2006; 5:525–535. [PubMed: 16713924]
11. Lees AJ, Hardy J, Revesz T. Parkinson's disease. *Lancet*. 2009; 373:2055–2066. [PubMed: 19524782]
12. Banerjee R, Starkov AA, Beal MF, Thomas B. Mitochondrial dysfunction in the limelight of Parkinson's disease pathogenesis. *Biochimica et biophysica acta*. 2009; 1792:651–663. [PubMed: 19059336]
13. Imai Y, Lu B. Mitochondrial dynamics and mitophagy in Parkinson's disease: disordered cellular power plant becomes a big deal in a major movement disorder. *Curr Opin Neurobiol*. 2011; 21:935–941. [PubMed: 22048001]
14. Springer W, Kahle PJ. Regulation of PINK1-Parkin-mediated mitophagy. *Autophagy*. 2011; 7:266–278. [PubMed: 21187721]
15. Jin SM, et al. Mitochondrial membrane potential regulates PINK1 import and proteolytic destabilization by PARL. *J Cell Biol*. 2010; 191:933–942. [PubMed: 21115803]
16. Greene AW, et al. Mitochondrial processing peptidase regulates PINK1 processing, import and Parkin recruitment. *EMBO Rep*. 2012; 13:378–385. [PubMed: 22354088]
17. Matsuda N, et al. PINK1 stabilized by mitochondrial depolarization recruits Parkin to damaged mitochondria and activates latent Parkin for mitophagy. *J Cell Biol*. 2010; 189:211–221. [PubMed: 20404107]
18. Vives-Bauza C, et al. PINK1-dependent recruitment of Parkin to mitochondria in mitophagy. *Proc Natl Acad Sci U S A*. 2010; 107:378–383. [PubMed: 19966284]
19. Valente EM, et al. Hereditary early-onset Parkinson's disease caused by mutations in PINK1. *Science*. 2004; 304:1158–1160. [PubMed: 15087508]
20. Nuytemans K, Theuns J, Cruts M, Van Broeckhoven C. Genetic etiology of Parkinson disease associated with mutations in the SNCA, PARK2, PINK1, PARK7, and LRRK2 genes: a mutation update. *Hum Mutat*. 2010; 31:763–780. [PubMed: 20506312]
21. Corti O, Lesage S, Brice A. What genetics tells us about the causes and mechanisms of Parkinson's disease. *Physiol Rev*. 2011; 91:1161–1218. [PubMed: 22013209]
22. Takeda K, et al. Mitochondrial phosphoglycerate mutase 5 uses alternate catalytic activity as a protein serine/threonine phosphatase to activate ASK1. *Proc Natl Acad Sci U S A*. 2009; 106:12301–12305. [PubMed: 19590015]
23. Lo SC, Hannink M. PGAM5, a Bcl-XL-interacting protein, is a novel substrate for the redox-regulated Keap1-dependent ubiquitin ligase complex. *J Biol Chem*. 2006; 281:37893–37903. [PubMed: 17046835]
24. Lo SC, Hannink M. PGAM5 tethers a ternary complex containing Keap1 and Nrf2 to mitochondria. *Exp Cell Res*. 2008; 314:1789–1803. [PubMed: 18387606]
25. Wang Z, Jiang H, Chen S, Du F, Wang X. The mitochondrial phosphatase PGAM5 functions at the convergence point of multiple necrotic death pathways. *Cell*. 2012; 148:228–243. [PubMed: 22265414]
26. Imai Y, et al. The loss of PGAM5 suppresses the mitochondrial degeneration caused by inactivation of PINK1 in *Drosophila*. *PLoS Genet*. 2010; 6:e1001229. [PubMed: 21151955]
27. Sekine S, et al. Rhomboid protease PARL mediates the mitochondrial membrane potential loss-induced cleavage of PGAM5. *J Biol Chem*. 2012; 287:34635–34645. [PubMed: 22915595]

28. Myeku N, Figueiredo-Pereira ME. Dynamics of the degradation of ubiquitinated proteins by proteasomes and autophagy: association with sequestosome 1/p62. *J Biol Chem*. 2011; 286:22426–22440. [PubMed: 21536669]
29. Katayama H, Kogure T, Mizushima N, Yoshimori T, Miyawaki A. A sensitive and quantitative technique for detecting autophagic events based on lysosomal delivery. *Chem Biol*. 2011; 18:1042–1052. [PubMed: 21867919]
30. Lorenz H, Hailey DW, Lippincott-Schwartz J. Addressing membrane protein topology using the fluorescence protease protection (FPP) assay. *Methods Mol Biol*. 2008; 440:227–233. [PubMed: 18369949]
31. Kitada T, et al. Impaired dopamine release and synaptic plasticity in the striatum of PINK1-deficient mice. *Proc Natl Acad Sci U S A*. 2007; 104:11441–11446. [PubMed: 17563363]
32. Gispert S, et al. Parkinson phenotype in aged PINK1-deficient mice is accompanied by progressive mitochondrial dysfunction in absence of neurodegeneration. *PLoS One*. 2009; 4:e5777. [PubMed: 19492057]
33. Taylor TN, Greene JG, Miller GW. Behavioral phenotyping of mouse models of Parkinson's disease. *Behav Brain Res*. 2010; 211:1–10. [PubMed: 20211655]
34. Brooks SP, Dunnett SB. Tests to assess motor phenotype in mice: a user's guide. *Nat Rev Neurosci*. 2009; 10:519–529. [PubMed: 19513088]
35. Billia F, et al. PTEN-inducible kinase 1 (PINK1)/Park6 is indispensable for normal heart function. *Proc Natl Acad Sci U S A*. 2011; 108(23):9572–7. [PubMed: 21606348]
36. Santos D, Cardoso SM. Mitochondrial dynamics and neuronal fate in Parkinson's disease. *Mitochondrion*. 2012; 12:428–437. [PubMed: 22609323]
37. Shin JH, et al. PARIS (ZNF746) repression of PGC-1 α contributes to neurodegeneration in Parkinson's disease. *Cell*. 2011; 144:689–702. [PubMed: 21376232]
38. Clark IE, et al. *Drosophila pink1* is required for mitochondrial function and interacts genetically with parkin. *Nature*. 2006; 441:1162–1166. [PubMed: 16672981]
39. Park J, et al. Mitochondrial dysfunction in *Drosophila* PINK1 mutants is complemented by parkin. *Nature*. 2006; 441:1157–1161. [PubMed: 16672980]
40. Bezard E, et al. Relationship between the appearance of symptoms and the level of nigrostriatal degeneration in a progressive 1-methyl-4-phenyl-1,2,3,6-tetrahydropyridine-lesioned macaque model of Parkinson's disease. *J Neurosci*. 2001; 21(17):6853–61. [PubMed: 11517273]
41. Hsiao EY, et al. Microbiota modulate behavioral and physiological abnormalities associated with neurodevelopmental disorders. *Cell*. 2013; 155(7):1451–63. [PubMed: 24315484]
42. Ivanov II, et al. Induction of intestinal Th17 cells by segmented filamentous bacteria. *Cell*. 2009; 139(3):485–98. [PubMed: 19836068]
43. Kumar V, et al. C57BL/6N mutation in cytoplasmic FMRP interacting protein 2 regulates cocaine response. *Science*. 2013; 342(6165):1508–12. [PubMed: 24357318]
44. Kayagaki N, et al. Non-canonical inflammasome activation targets caspase-11. *Nature*. 2011; 479(7371):117–21. [PubMed: 22002608]
45. Farrer MJ. Genetics of Parkinson disease: paradigm shifts and future prospects. *Nat Rev Genet*. 2006; 7:306–318. [PubMed: 16543934]
46. Wang X, Michaelis EK. Selective neuronal vulnerability to oxidative stress in the brain. *Front Aging Neurosci*. 2010; 2:12. [PubMed: 20552050]
47. Vincelette J, et al. Gait analysis in a murine model of collagen-induced arthritis. *Arthritis Res Ther*. 2007; 9:R123. [PubMed: 18036238]
48. Piesla MJ, et al. Abnormal gait, due to inflammation but not nerve injury, reflects enhanced nociception in preclinical pain models. *Brain Res*. 2009; 1295:89–98. [PubMed: 19651113]
49. Matsuura K, Kabuto H, Makino H, Ogawa N. Pole test is a useful method for evaluating the mouse movement disorder caused by striatal dopamine depletion. *J Neurosci Methods*. 1997; 73:45–48. [PubMed: 9130677]
50. Lee Y, et al. Parthanatos mediates AIMP2-activated age-dependent dopaminergic neuronal loss. *Nat Neurosci*. 2013; 16:1392–1400. [PubMed: 23974709]

51. Hwang DY, et al. 3,4-dihydroxyphenylalanine reverses the motor deficits in Pitx3-deficient aphakia mice: behavioral characterization of a novel genetic model of Parkinson's disease. *J Neurosci.* 2005; 25(8):2132–7. [PubMed: 15728853]

Author Manuscript

Author Manuscript

Author Manuscript

Author Manuscript

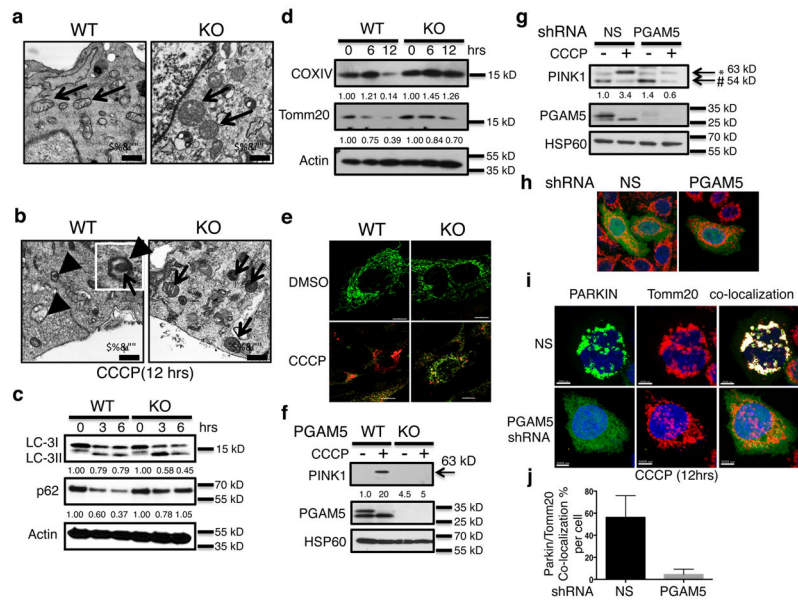


Fig. 1. PGAM5 is required for PINK1-triggered mitophagy

(a) WT and *Pgam5* KO MEFs evaluated by TEM. The black arrows indicate mitochondria; (b) TEM analysis after 12 hours CCCP treatment; black arrowheads indicate double-membrane structures (DMS). Inset shows a DMS with an encapsulated mitochondrion. The black arrows indicate mitochondria. Size bar = 0.5 micron; (c) WT and KO MEFs were treated with CCCP for 0, 3 or 6 hr and cytosolic fractions were immunoblotted with anti-LC3, anti-p62, or anti-actin as indicated. (d) Similar to (c), treated with CCCP for 6 and 12 hr and immunoblotted for anti-COXIV, anti-Tomm20, or anti-actin as indicated. For c. and d., the numbers below each lane indicate the fractional band density compared to the 0 hrs time point which has been set at 1.0; (e) Confocal photomicrographs of mtKeima-transduced WT and KO MEFs treated with CCCP or DMSO vehicle for 12 hrs (6 individual cells from each group were scanned and representative cells are shown); Intracellular mt-Keima excited at 450nm was shown in green color, while red color indicated the excitation by 550nm in the same cell. (f) Mitochondrial extracts of WT and *Pgam5* KO MEFs treated with DMSO (-) or CCCP (+) for 3 hours and analyzed by immunoblot as above. (Note that mouse PINK1 antibody can only detect the full length PINK1). Arrow indicates the 63 kD form of PINK1. (g) HeLa cells transfected with either nonspecific (NS) or PGAM5 short hairpin RNA viruses (shRNA) were treated with CCCP for 3 hours, and mitochondrial fractions were immunoblotted for the proteins indicated. Full-length (*63kD) and cleaved (#54kD) PINK1 are indicated. For f. and g., the numbers below indicate the Full-length PINK1 band density compared to the first lane which has been set at 1.0 (h) Confocal micrographs of HeLa cells as in g. were transfected with PARKIN-YFP (Green) plasmid before CCCP treatment, then (i) treated with CCCP for 12 hours. Mitochondria were stained with anti-Tomm20 (Red) Dapi stained nuclear was shown in blue. Colocalization was indicated by white color. (j) Quantification of the colocalization percentage of Tomm20 (Red) with parkin (Green) per cell by Imaris software (n=7 for NS and *PGAM5* shRNA group separately. Results are presented as mean and standard deviations and were analyzed

by the student t -test). All the blots and images are from representative of three independent experiments.

Author Manuscript

Author Manuscript

Author Manuscript

Author Manuscript

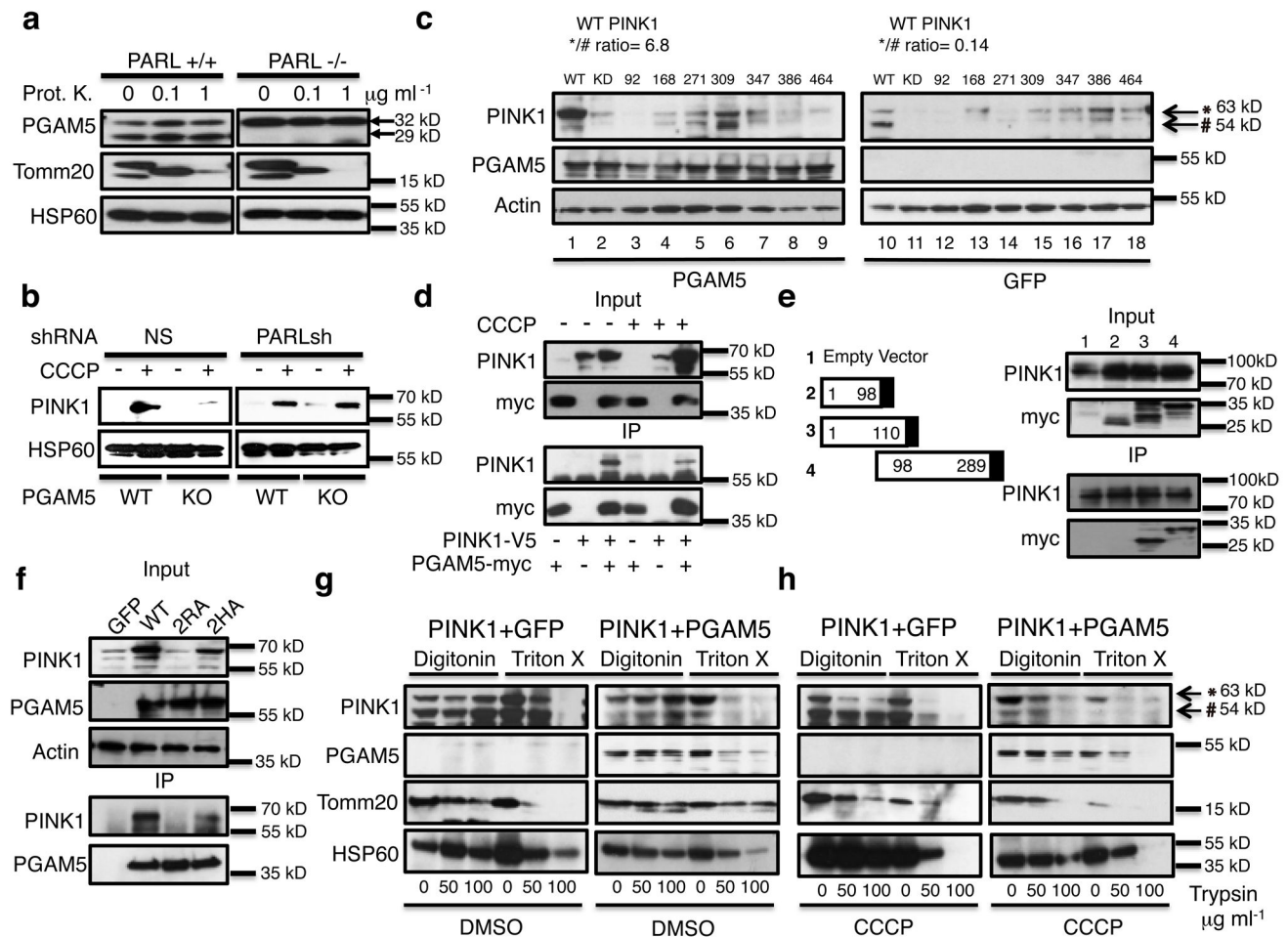


Fig. 2. PGAM5 stabilizes PINK1 in mitochondria

(a) Mitochondria from MEFs from *Parl* WT (+/+) and KO (-/-) mice were treated with the indicated doses of proteinase K (Prot.K) for 30 minutes on ice and then immunoblotted for the indicated proteins. Full-length and cleaved PGAM5 bands are indicated with arrows. (b) *Pgam5* WT and KO MEFs were transduced with either nonspecific (NS) or *Parl* short hairpin RNA viruses (shRNA) and either treated (+) or not (-) with CCCP for 3 hours. Mitochondria were then purified and analyzed by immunoblot for the indicated proteins. (c) WT PINK1 as well as kinase dead (KD) or Parkinson's disease-associated PINK1 mutants (C92F, A168P, H271Q, G309D, L347P, G386S, R464H) were co-transfected into HEK293T cells with the same amount PGAM5 (lane 1-9) or GFP (lane 10-18) expression plasmids and total cell lysates were immunoblotting for PINK1, PGAM5, and actin. The ratio of WT full-length (63kD) versus cleaved (54kD) PINK1 (*/#) is shown. (d) Anti-myc immunoprecipitates (IP) of lysates from 293T cells transfected with combinations of myc-tagged PGAM5 and PINK1-V5 with or without CCCP treatment and immunoblotting with anti-PINK1 or anti-myc. (e) Four constructs expressing either: 1. no PGAM5 (empty vector) or 2. amino acids 1-98, 3. 1-110, and 4. 98-289 truncated versions of PGAM5 (left panel). Immunoblot of HEK293T cells expressing PINK1-GFP and myc-tagged PGAM5 truncation mutants as indicated with anti-PINK1 or anti-myc for the input proteins as well as the anti-

GFP immunoprecipitates (IP)(right panel). (f) Co-transfection of GFP, WT PGAM5, 2RA mutant (R98A and R104A) or the 2HA mutant (H99A and H105A) with a PINK1 expression plasmid into HEK293T cells and the input cell lysates as well as the anti-myc immunoprecipitates (IP) were immunoblotted with antibodies against PINK1, PGAM5, or actin. WT PINK1 was expressed in HEK293T cells with or without PGAM5 or a GFP control plasmid after (g) DMSO or (h) CCCP treatment. Cells were permeabilized with digitonin or Triton X-100 separately, followed by treatment with the indicated amounts of trypsin on ice for 30 minutes. Cell lysates were immunoblotted for PINK1, PGAM5, Tomm20, or HSP60 as indicated. Full-length (*63kD) and cleaved (#54kD) PINK1 are shown.

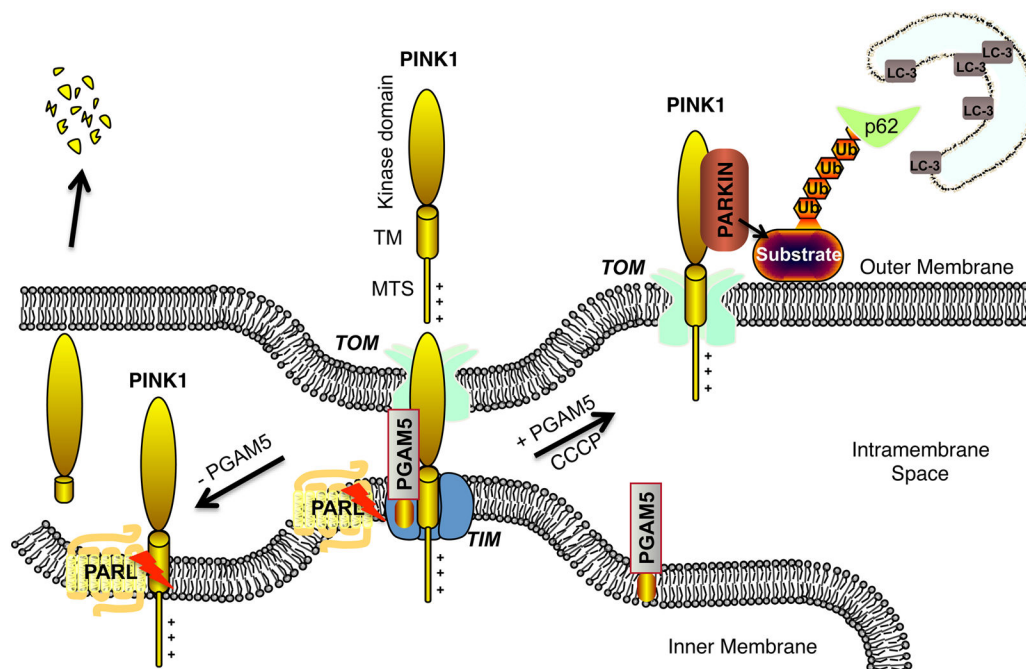


Fig. 3. Inside-Out PINK1 translocation model

PGAM5 is a mitochondria inner membrane (IMM) protein that protects PINK1 from degradation by mitochondrial proteases including PARL. After CCCP treatment, full-length PINK1 protected by PGAM5 will move to the mitochondria outer membrane (OMM), while PGAM5 remains on the IMM. In the absence of PGAM5, PINK1 loses the protection from PGAM5, and will be cleaved and degraded. CCCP can trigger PGAM5 stabilized PINK1 translocation from IMM to OMM where it associates with parkin leading to ubiquitination (Ub) events associated with p62 recruitment and culminating in LC-3-mediated mitophagy.

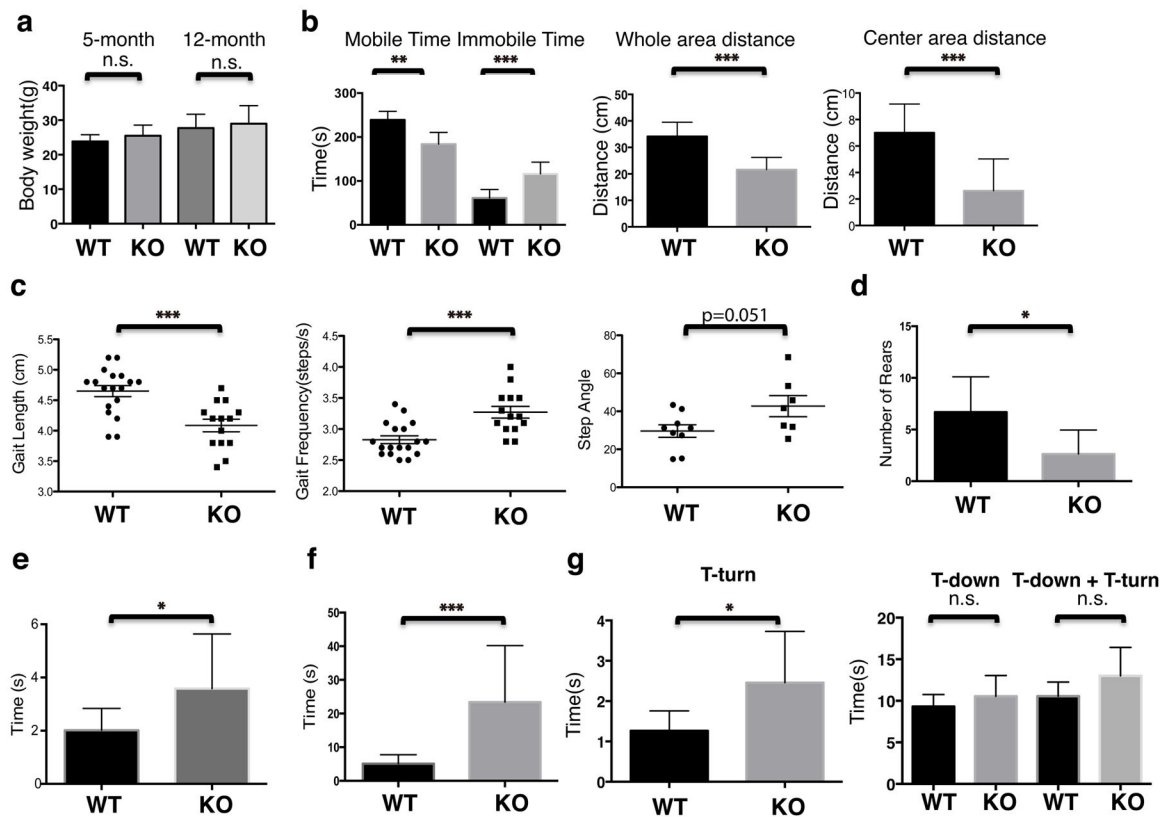


Fig. 4. Aged *Pgam5* KO mice show a Parkinson's disease-like phenotype

(a) Body weight was measured in 5-month old and 12-month old female *Pgam5* wild type (WT) and knockout (KO) mice. Behavioral measurements on 12-month old female WT and KO mice (WT n=10, KO n=8) were: (b) Open field tests including time spent mobile, time spent immobile, whole area distance, and center area distance; (c) Gait length, gait frequency in steps/second (s), and step angle; (d) rearing test, (e) akinesia test, and (f) ladder climb test, and (g) vertical pole test. T-turn indicates the time mice spent to turn their bodies 180 degrees from the head up start position prior to descending the pole. T-down indicates the time mice spent to descend to the bottom of pole. Graphs show the mean and standard deviations and were analyzed by the student t test, * $P < 0.05$, ** $P < 0.01$, *** $P < 0.001$, n.s. = not significant.

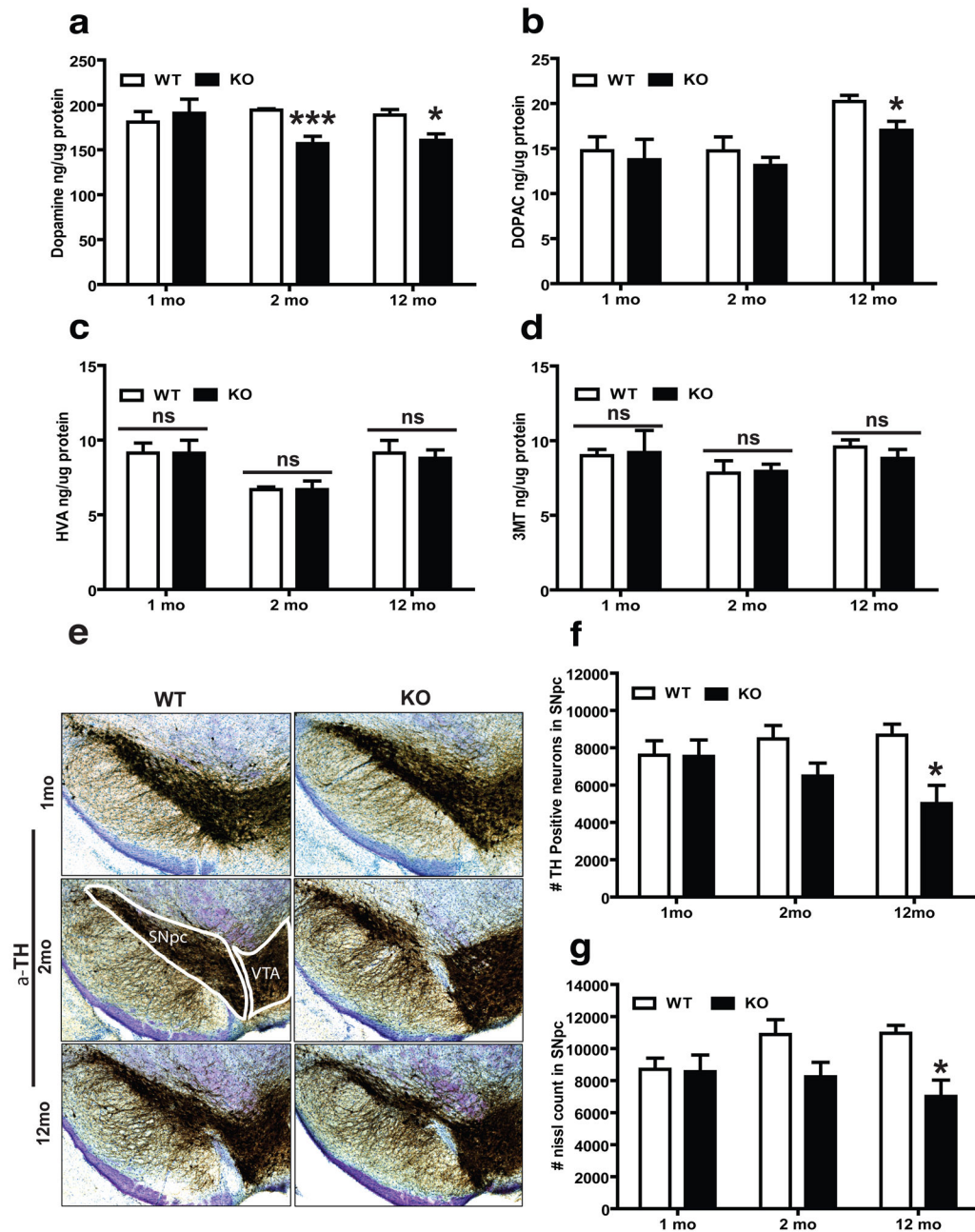


Fig. 5. *Pgam5* KO mice show progressive dopaminergic neurodegeneration

HPLC-ECD quantitation of (a) striatal DA and its metabolites (b) DOPAC (c) HVA and (d) 3MT levels at three different time points (1-month, 2-month old and 12-month old) in *Pgam5* wild type (WT) or knockout (KO) mice. In 1, 2 and 12 mo cohorts, TH-positive neurons were quantified in the substantia nigra pars compacta (SNpc) region of WT and KO mice by unbiased stereological counting. (e) Representative images of TH-immunohistochemistry from WT and KO mice. The ventral tegmental area (VTA) region is indicated. Stereological quantitation of (f) TH and (g) Nissl-positive neurons in the SNpc (*n*

= 4 mice per group). Error bars represent the mean \pm standard error of the mean, $n=4$ mice per group. (two-way ANOVA, *** $P<0.01$, * $P<0.05$, ns = not significant)

Author Manuscript

Author Manuscript

Author Manuscript

Author Manuscript

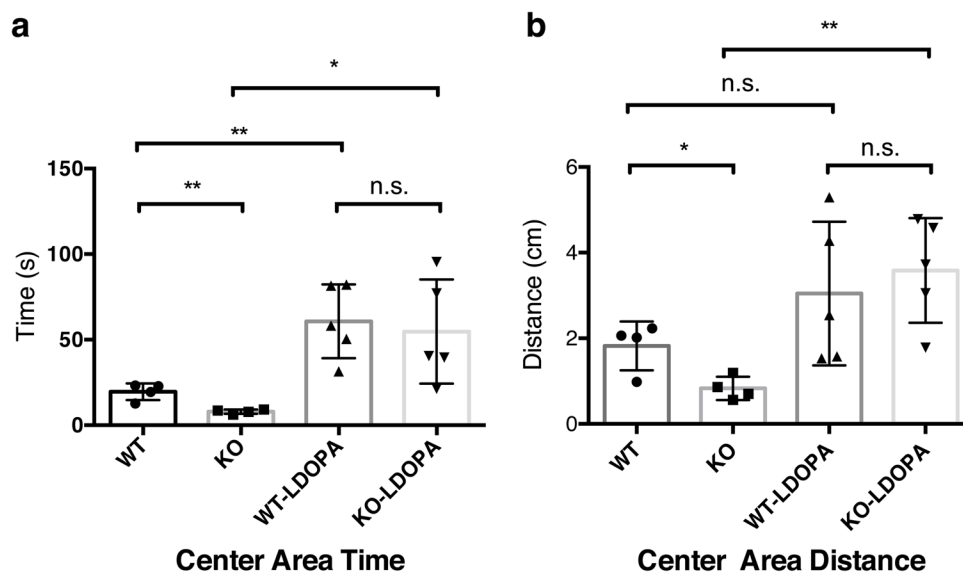


Fig. 6. L-DOPA rescues the abnormal behavior phenotype in KO mice

18-month old female *Pgam5* WT and KO mice received either water as control ($n = 4$), or 5 mg kg^{-1} L-DOPA and 12.5 mg kg^{-1} Benserazide ($n = 5$) by intraperitoneal injection.

Twenty minutes later, mice were subjected to the Open-Field-Test and the center area time in seconds (s) as well as the center area distance in centimeters (cm) were measured as described in the Materials and Methods. Graphs show the mean and standard deviations and were analyzed by the student *t*-test, n.s. no significance; * $P < 0.05$; ** $P < 0.01$.